J. Integr. Sci. Technol. 2021, 9(2), 98-106 Article

Journal of Integrated
SCIENCE & TECHNOLOGY

Defected Top diamond shaped Patch Antenna for Multi-Band operations

Rahmani Naveed Akhtar,[1*] Anupama A. Deshpande,[1] A. K. Kureshi[2]

[1]Department of Electronics And Communication Engineering, Shri Jagdishprasad Jhabarmal Tibrewala University, Rajasthan, India. [2]M. H. SabooSiddik Polytechnic, Mumbai, INDIA

Received on: 12-Oct-2021, Accepted and Published on: 04-Dec-2021

ABSTRACT

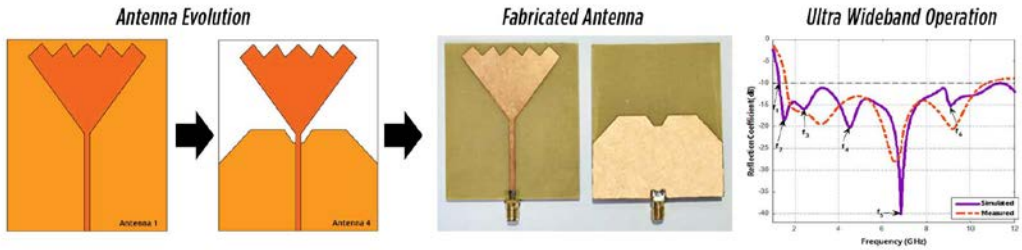

A compact diamond-shaped antenna has been presented in this research work. This antenna has been designed to cover multiple technologies like WLAN, Wi-MAX, Bluetooth and applications included in S-band, C-band and X-Bands. The proposed antenna design has a diamond-shaped patch with half ground structure with notch and side cuts to achieve more efficient radiation patterns, and characteristic impedance is achieved. The presented antenna has dimensions 60×71.5×1.6 mm^3, and the substrate is made of FR-4 material. The novel design and ground defections have achieved the proposed antenna's wider operational impedance bandwidth of 9.954 GHz. In addition, its frequency bandwidth with VSWR<2 is from 1.294 GHz to 11.248 GHz, which covers multiple technologies like 5G networks, WLAN, Wi-MAX, Bluetooth, satellite and applications included in S-band, C-band and X-Bands or ultra-wideband (UWB). The optimized simulated geometry has a good match with the measured outcomes.

Keywords: 5G, MSPA, UWB, WiMAX, S-band, C-band and X-Bands

INTRODUCTION

Wireless Communication is a bridge to connect next-generation innovations. Most of them will be facilitated by modern wireless technologies, Internet of Things (IoT) enabled. Antennas are the most constructive part of achieving quality communications. Today, communication needs more extensive bandwidth to target multiple technologies through a single antenna. To fulfil bandwidth necessities, more comprehensive bandwidth antennas are required. Due to the increase in never-ending demand in capacity and speed, one has to use a broader spectrum in the range of 3.1 to 10.6 GHz assigned by the Federal Communications Commission (FCC) in 2002 for UWB systems.[1] Table 1 illustrates the breakdown of the significant frequency applications used in ultra-wideband (UWB) networks.

The challenges in using UWB in consumer applications are that the frequency band is susceptible to interference with existing wireless systems. For example, the IEEE 802.16 standard for WiMAX system at 3.5 GHz (3.3-3.7 GHz) and the IEEE 802.11a standard for WLAN system at 5.5 GHz (5.15-5.825 GHz) as shown in Table 1. In standard working scenarios, antennas should be designed as specific frequency bands. Incorporating multiple bands has excellent bandwidth, and broader operating frequency applications impact the antenna's gain. Nevertheless, the versatility of the antenna is also a significant factor in the research. Some UWB antennas have been recently designed.[2-3]

In this work, the microstrip patch antenna is utilized to plan at 5G applications since it has magnetic elements like low profile, lightweight, tiny in size, simplicity of manufacture, and incorporation with different devices. In this design, escalated examinations are carried on microstrip patch antennas to upgrade more extensive impedance bandwidth in wireless communication

*Rahmani Naveed Akhtar, Department of Electronics and Communication Engineering, Shri Jagdishprasad Jhabarmal Tibrewala University, Rajasthan, India.
Email: rahmaninaveed2021@gmail.com

Cite as: *J. Integr. Sci. Technol., 2021, 9(2), 98-106.*

 ISSN: 2321-4635 http://pubs.iscience.in/jist

for multiple applications. Here, the materials are viewed as Flame Retardant-4 (FR-4) to accomplish more extensive impedance bandwidth with streamlined construction utilizing electromagnetic simulation devices.

Table 1. UWB Frequencies Applications

Frequency	Technology/Application
1.6 GHz	GPS
1.9 GHz	PCS
2.4 GHz	Bluetooth, Wi-Fi, IEEE 802.11b
3.3 – 3.7 GHz	WiMAX
5 GHz	Wi-Fi, IEEE 802.11a
6.25 GHz	Satellite
7.725-8.275 GHz	ITU
3.1 GHz – 10.6 GHz	UWB Spectrum

Analysis and Design of the Antenna

Impedance matching of antenna is essential while designing its geometry, with the good matching of impedance results in efficient power transfer that is why the antenna was made. The improper or mismatched antenna impedance creates unnecessary signals reflecting the source and creates standing waves, often called voltage standing wave ratio (VSWR) and higher reflection coefficient or return loss $-|S_{11}|$. For the adequately matched antennas, VSWR is below two and return loss should be below -10dB. These are the most primary factor for the get design and efficient antenna. Other factors are considered but usually kept secondary, like gain, directivity, and radiation efficiencies.

During the design process, the motive of the work is to design such an antenna that covers a more significant number of applications instead of focussing on any specific application band.

Antenna Evolution

The final antenna geometry has been achieved after many design upgrades. Figures 1(a) to (d) have shown these antenna designs.

Figure 1 shows four antennas; the last one (Antenna 4) is the optimized version of previous designs. Antenna 1 has whole ground and a diamond-shaped patch with a 50 ohms feedline. The return loss characteristics of Antenna 1 are shown in Figure 2 as a yellow curve. The return loss of the antenna was so much higher and only below -10dB on 3.619 GHz, 6.049 GHz, 8.2 GHz and 9.136 GHz with a very narrow band.

In Antenna 2, the ground plane has cut down to nearly half of the antenna length near the joint of the patch and feedline. The return loss characteristics due to this cut in the ground were decreased below -10 dB, and two bands were formed that can be seen in Figure 2 with the blue curve. The first band was created between 1.2782 GHz to 2.3551 GHz, and the second band was between 4.21 GHz and 10 GHz. This design was good in performance but not fulfilled our aim so that further changes in the design has been made.

In Antenna 3, a notch is created opposite to the patch and feedline joint. Due to this, the previous band (Antenna 2) has been increased and created two-band again having better return loss (see Figure 2 orange curve). The first band is between 1.33 GHz and 2.62 GHz, and the second is between 3.39 GHz and 9.79 GHz.

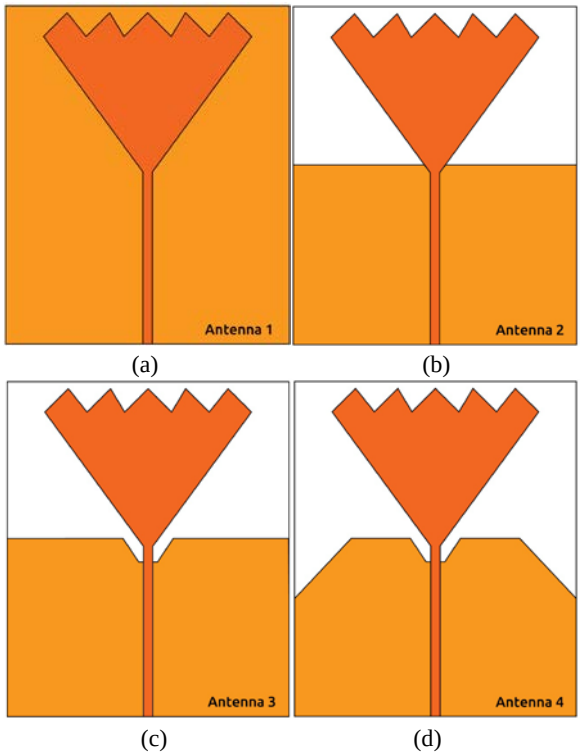

Figure 1. Evolution of Proposed Antenna (a) Antenna 1, (b) Antenna 2, (c) Antenna 3, (d) Antenna 4 (Final design)

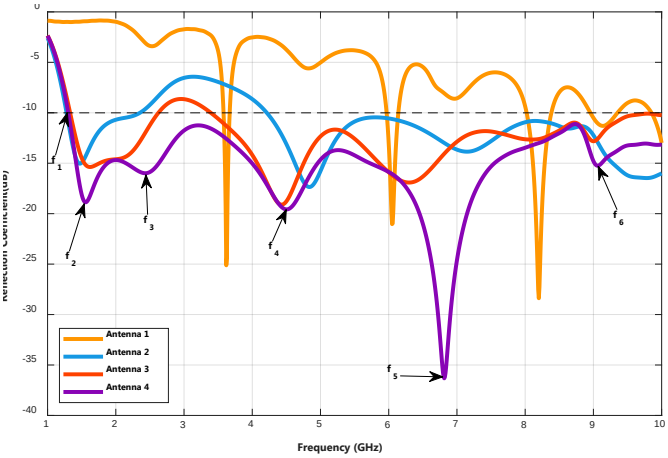

Figure 2. Comparison of Antenna Return Loss Characteristics of Antennas 1 to 4

These return loss characteristics are better than the previous design but do not have ultra-wide bandwidth. So, more optimization has been done.

In Antenna 4, the ground structure is further defected by symmetrical slant cuts along with the side corners of the antenna ground. As a result, antenna bandwidth has been created, and return loss of antenna has been decreased further down to -37.71 dB on 6.838 GHz. Now the antenna operating band is between 1.294 GHz and 11.248 GHz. Where 1.294 GHz is the lower cut off frequency, and 11.248 GHz are the higher cut off frequency. These characteristics have been shown in Figure 2 with the purple coloured curve. Table 2 shows the different frequencies (lower cut-off, higher cut-off and resonance).

Table 2: Proposed Antenna Frequencies

Frequencies	Label	Values	Return Loss
Lower Cutoff	f_L	1.294 GHz	-10.000 dB
Higher Cutoff	f_H	11.248 GHz	-10.000 dB
Resonating Frequencies	fr_1	1.532 GHz	-18.500 dB
	fr_2	2.414 GHz	-15.850 dB
	fr_3	4.500 GHz	-20.121 dB
	fr_4	6.838 GHz	-40.033 dB
	fr_5	9.078 GHz	-15.282 dB

Proposed Optimized Antenna Dimension

The antenna geometry and dimensions of the proposed monopole antenna are shown in Figure 3. The detailed antenna dimensions of the proposed antenna have been shown in Table 3.

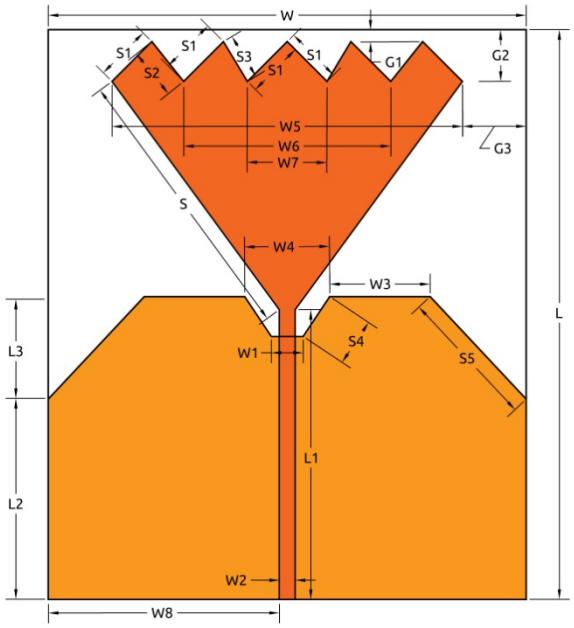

Figure 3. Antenna dimensions of the proposed diamond-shaped monopole antenna

Table 3. Proposed antenna dimensions

Dimension	Values	Dimension	Values
W	60 mm	W_7	10 mm
W_1	4 mm	W_8	29 mm
W_2	2 mm	L	71.5 mm
W_3	12.6 mm	L_1	36.36 mm
W_4	10.66 mm	L_2	25.2 mm
W_5	44 mm	L_3	12.45 mm
W_6	26 mm	S_1	7.07 mm
S_2	6.40 mm	G_1	1.5 mm
S_3	5.83 mm	G_2	6.46 mm
S_4	5.34 mm	G_3	8 mm
S_5	17.64 mm		

Experimental Results and Discussion

Reflection Coefficient Characteristics

The reflection coefficient characteristics of the proposed diamond-shaped antenna show a simulated fractional bandwidth of 147% with a lower cut-off frequency of 1.294 GHz and a higher cut-off frequency of 11.248 GHz. The fabricated proposed monopole antenna is shown in Figure 4(a). The antenna has been tested, and measured return loss has been compared with simulated return loss (refer to Figure 4(b)).

Table 4. Comparison of simulated and measured results of the proposed antenna

Mode	Resonant Frequency (GHz)	Reflection Coefficient (dB)	Impedance Bandwidth (GHz)	BW (%)
Simulated	1.532 GHz	-18.500 dB	9.954 GHz	147
	2.414 GHz	-15.850 dB		
	4.500 GHz	-20.121 dB		
	6.838 GHz	-40.033 dB		
	9.078 GHz	-15.282 dB		
Measured	3.19 GHz	-19.41 dB	9.11 GHz	147.88
	6.55 GHz	-28.03 dB		
	9.17 GHz	-20.51 dB		

The measured results are obtained from Network Analyzer and found that the lower cut-off frequency is 1.61 GHz, and the higher cut-off frequency is 10.72 GHz, having bandwidth 9.11 GHz and measured fractional bandwidth 147.88% for $|S_{11}| < -10$dB calculated with Equation (1).

From simulated and measured return loss (S_{11}) analysis, it is clear that the measured performance of the antenna is nearer to simulated performance, and the antenna will work as per the research goal of this work.

Calculation of Fractional Bandwidth

The fractional bandwidth of the proposed diamond-shaped antenna is calculated using Equation (1). The simulated results antenna has provided the fractional bandwidth of 147% and measured 147.88%.

$$FBW = 2 \times \frac{f_H - f_L}{f_H + f_L} \times 100\ \% \quad \ldots (1)$$

$$= 2 \times \frac{11.248 - 1.294}{11.248 + 1.294} \times 100\ \%$$

$$= 2 \times \left(\frac{9.954}{13.542}\right) \times 100\ \%$$

$$FBW = 147\ \%$$

Resonating Frequencies

The proposed antenna resonates on five frequencies 1.532 GHz, 2.414 GHz, 4.500 GHz, 6.838 GHz, and 9.078 GHz. The measured

resonant frequencies are only three and slightly differ from simulated frequencies 3.19 GHz, 6.55 GHz, and 9.17 GHz. The difference between simulated return loss characteristics and measured return loss characteristics are due to connector losses, conductor losses, interference and dielectric constant.

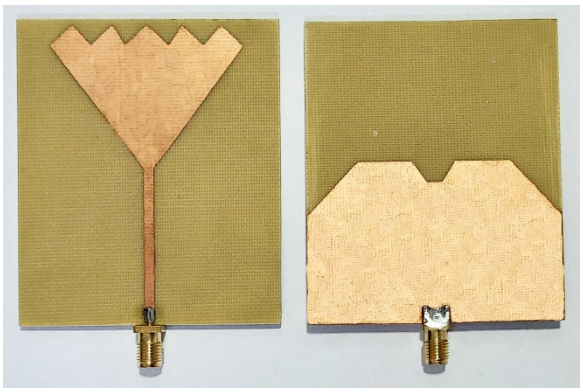

(a)

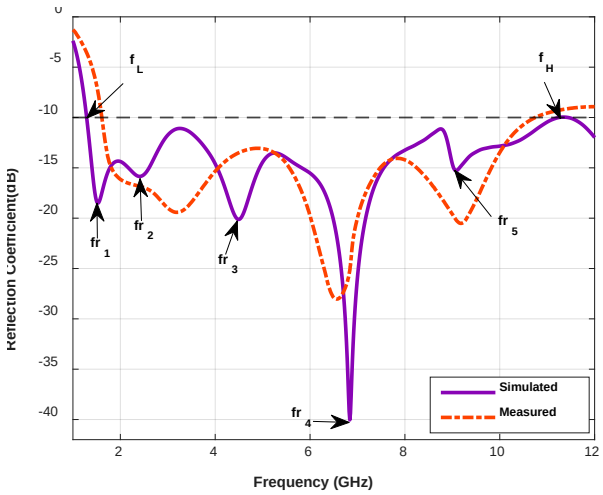

(b)

Figure 4. Proposed monopole antenna (a) Fabricated antenna (b) Comparison of Simulation vs Measured Return Loss

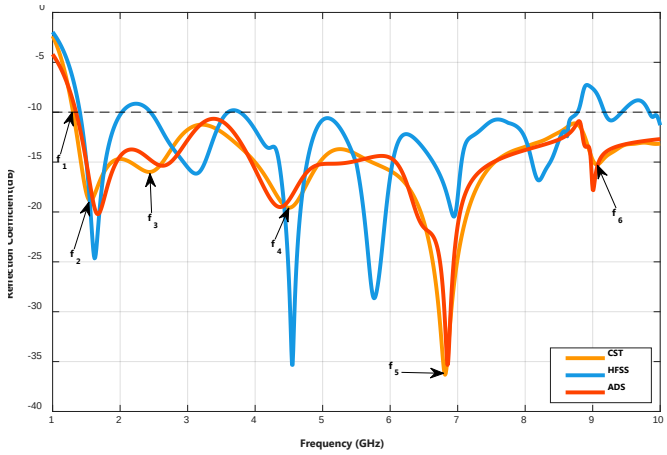

Figure 5. Reflection Coefficient of CST vs ADS vs HFSS

Further to get more clarity on the antenna's performance, the proposed design has been tested on different simulation tools like ADS and HFSS apart from CST. Figure 5 shows the reflection coefficient comparison of CST, HFSS and ADS. This comparison verified the proposed antennas performance and found a slight difference between them which is evident due to their electromagnetic simulation algorithms.

Impact of Notch Position (Ny)

To see the impact of a notch formed on the ground plane on the performance of the antenna. A parametric analysis has been performed on notch position along with the y-axis, parameter symbolized as Ny. This parameter has been varied from 0 to 3 mm with a step size of 0.5 mm. The return loss characteristics are shown and compared in Figure 6. The antenna notch has been shifted along with the antenna ground top edge towards the positive y-axis, and as it moves, the return loss of the antenna get decreases to 1.5 mm. However, when it shifts more than 1.5mm antenna start creating two bands instead of one single wideband. The best return loss got on value Ny=1, where the antenna's bandwidth is largest. The return loss for all values of Ny has been shown and compared in Figure 6, and the dotted curve with orange colour is the optimal curve of the antenna.

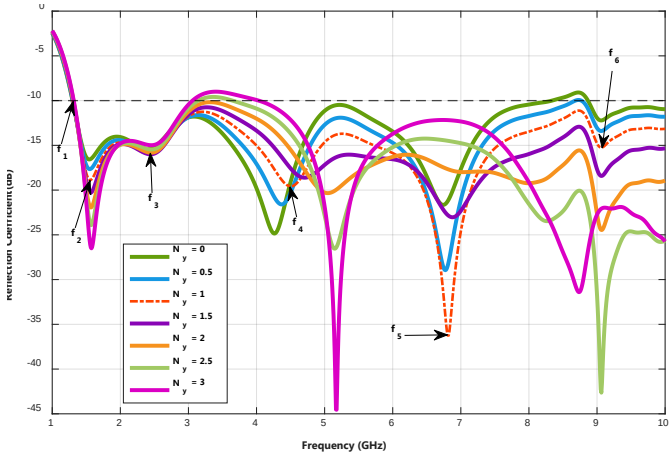

Figure 6. Notch Shift Parametric Outcomes for Return Loss

Surface Current Distribution

After exciting the antenna with the power, the current flows throughout the antenna. The current vectors show the amount of current in a particular place. The red colour shows the higher intensities, and the blue colour shows the lower intensities of the current.

The proposed diamond-shaped antenna has been evaluated for surface current distribution on resonant frequencies and presented in Figure 7. With the help of the current distribution analysis, we can find out the different parts of the antenna responsible for the radiation of signals.

Higher the intensity of current more radiation will be generated from that part of the antenna of some frequency. Stronger signals will create dips in return loss characteristics, and the lowest point of that dip is called centre frequency, which is called resonating frequency. Dips in return loss characteristics are called resonance frequencies. The current path can be evaluated theoretically using Equation (2).

$$f_r = \frac{c}{P\sqrt{\varepsilon_r}} \quad \ldots (2)$$

Where,

f_r = Resonance Frequency

c = Speed of Light

P = Path length

ε_r = Effective Dielectric Constant

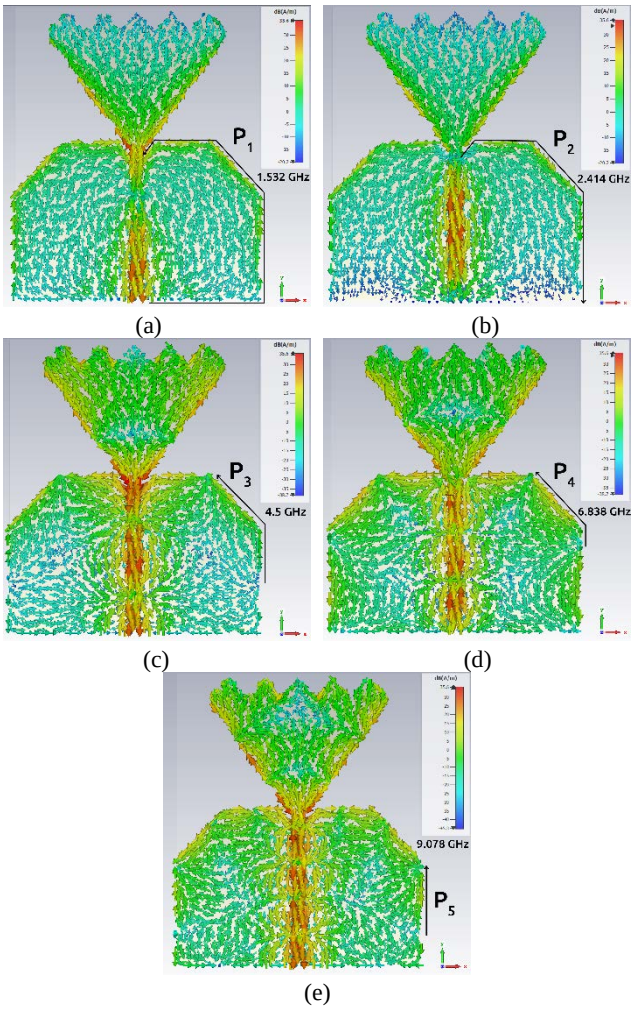

Figure 7: Surface current distribution of proposed diamond-shaped antenna on (a) 1.532 GHz, (b) 2.414 GHz, (c) 4.5 GHz, (d) 6.838 GHz, and (e) 9.078 GHz

Evaluation of First Resonance (1.532 GHz)

For theoretical evaluation of resonating frequency path, P_1 shown in Figure 7(a) is responsible for radiation, and the evaluated resonance frequency (fr_1) is 1.63 GHz. P_1 calculated using equation (3). From the simulated results, the resonating frequency is 1.532 GHz. The error is 6.3% between simulated and theoretical due to environmental and other losses.

$$P_1 = W_8+L_2+S_5+W_3+S_4+W_1/2 \quad \ldots (3)$$
$$= 29 + 25.2 + 17.64 + 12.6 + 5.34 + 2$$
$$= 91.78\ mm$$

Using Equation (2),

$$fr_1 = 1.63\ GHz \quad \ldots (4)$$

Evaluation of Second Resonance (2.414 GHz)

For theoretical evaluation of resonating frequency, path P_2 shown in Figure 7(b) is responsible for radiation, and the evaluated resonance frequency (fr_2) is 2.466 GHz. P_2 calculated using equation (5). From the simulated results, the resonating frequency is 2.414 GHz. The error is 5.2% between simulated and theoretical due to environmental and other losses.

$$P_2 = S_4+W_3+S_5+L_2 \quad \ldots (5)$$
$$= 5.34 + 12.6 + 17.64 + 25.2$$
$$= 60.78\ mm$$

Using Equation (2),

$$fr_2 = 2.466\ GHz \quad \ldots (6)$$

Evaluation of Third Resonance (4.5 GHz)

For theoretical evaluation of resonating frequency path, P_3 shown in Figure 7(c) is responsible for radiation, and the evaluated resonance frequency (fr_3) is 4.95 GHz. P_3 calculated using equation (7). From the simulated results, the resonating frequency is 4.5 GHz. The error is 10% between simulated and theoretical due to environmental and other losses.

$$P_3 = (L_2/2) + S_5 \quad \ldots (7)$$
$$= 12.6 + 17.64$$
$$= 30.24\ mm$$

Using Equation (2),

$$fr_3 = 4.95\ GHz \quad \ldots (8)$$

Evaluation of Fourth Resonance (6.838 GHz)

For theoretical evaluation of resonating frequency path, P_4 shown in Figure 7(d) is responsible for radiation, and the evaluated resonance frequency (fr_4) is 6.26 GHz. P_4 calculated using equation (9). From the simulated results, the resonating frequency is 6.838 GHz. The error is 8.4% between simulated and theoretical due to environmental and other losses.

$$P_4 = S_5+ L_2/4 \quad \ldots (9)$$
$$= 17.64 + 6.3$$
$$= 23.94\ mm$$

Using Equation (2),

$$fr_4 = 6.26\ GHz \quad \ldots (10)$$

Evaluation of Fifth Resonance (9.078 GHz)

For theoretical evaluation of resonating frequency path, P_5 shown in Figure 7(e) is responsible for radiation, and the evaluated resonance frequency (fr_5) is 8.92 GHz. P_5 was calculated using equation (11). From the simulated results, the resonating frequency is 9.078 GHz. The error is 1.74% between simulated and theoretical due to environmental and other losses.

$$P_5 = 0.66 \times L_2 \quad \ldots (11)$$
$$= 0.66 \times 25.2$$
$$= 16.8\ mm$$

Using Equation (2),

$$fr_5 = 8.92\ GHz \quad \ldots (12)$$

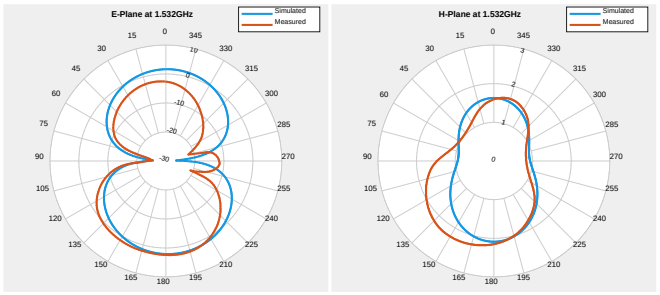

(a)

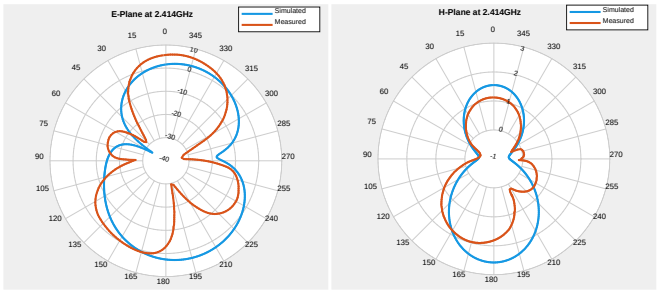

(b)

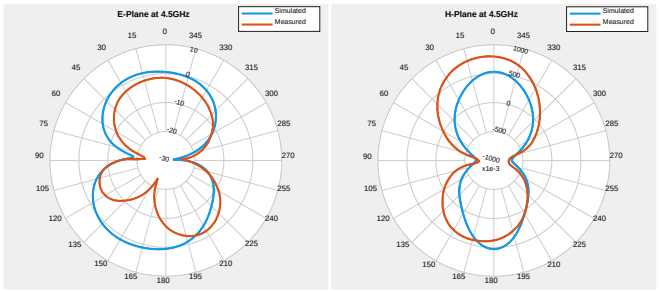

(c)

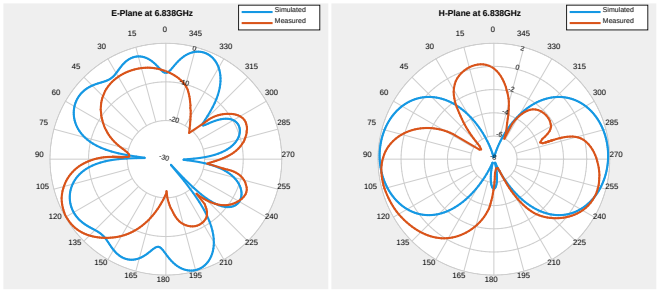

(d)

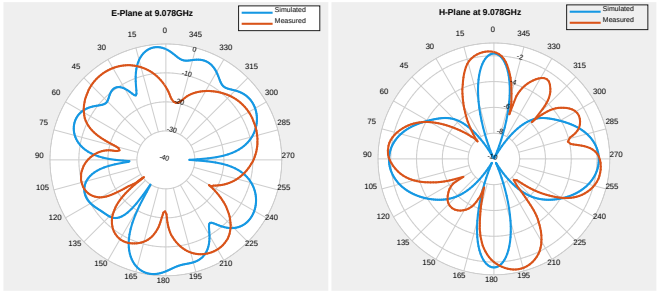

(e)

Figure 8. 2D Far-Field Results of E-plane and H-plane respectively on (a) 1.532 GHz, (b) 2.414 GHz, (c) 4.500 GHz, (d) 6.838 GHz, and (e) 9.078 GHz

The surface current distribution of the antenna and its different resonating frequencies are compared with simulated results and the percentage difference shown in Table 5. The maximum difference between theoretical and simulated values is 10%, and the minimum is 1.74%.

Table 5. Comparison of simulated and theoretical resonance frequencies

Freq. Label	Simulated Resonance Freq. (GHz)	Evaluated Resonance Frequency	Current Path Label	Current Path Length Responsible (mm)	Error (%)
fr_1	1.532	1.63	P_1	91.78	6.3
fr_2	2.414	2.46	P_2	60.78	5.2
fr_3	4.5	4.95	P_3	30.24	10
fr_4	6.838	6.26	P_4	23.94	8.4
fr_5	9.078	8.92	P_5	16.80	1.74

2D Far-field Analysis

The analysis between simulated and measured far-field radiation patterns results have been achieved and found slightly vary due to surrounding environment of measuring instruments or fabrication error (refer Figure 8). At the resonating frequencies 1.532 GHz, 2.414 GHz, 4.500 GHz, 6.838 GHz, and 9.078 GHz, a Far-field pattern has been found Omni-directional in E-Plane and H-Plane.

Input Impedance

The input impedance of the designed antenna is presented in Figure 9. It is observed that the multiple loops are found inside the VSWR circle indicates the mutual coupling and overlapping between resonating modes, which are essential for wide impedance bandwidth (refer to Figure 10).

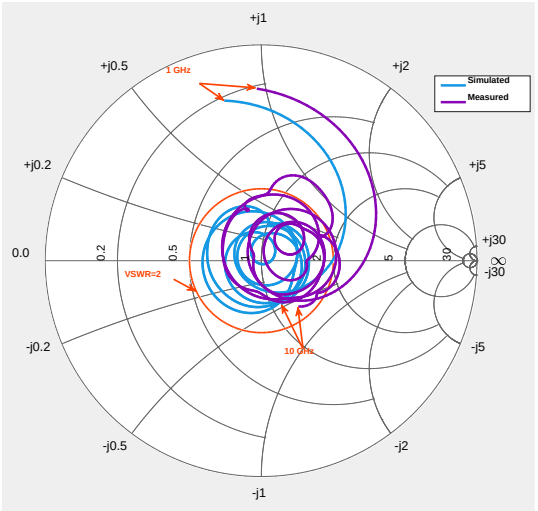

Figure 9. Impedance Curve

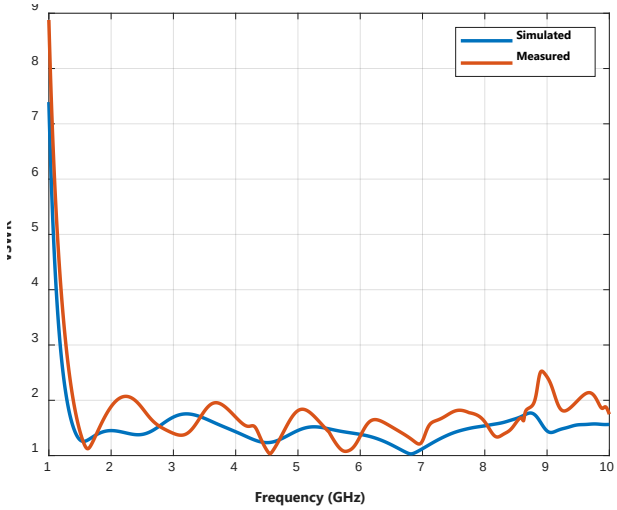

Figure 10. VSWR

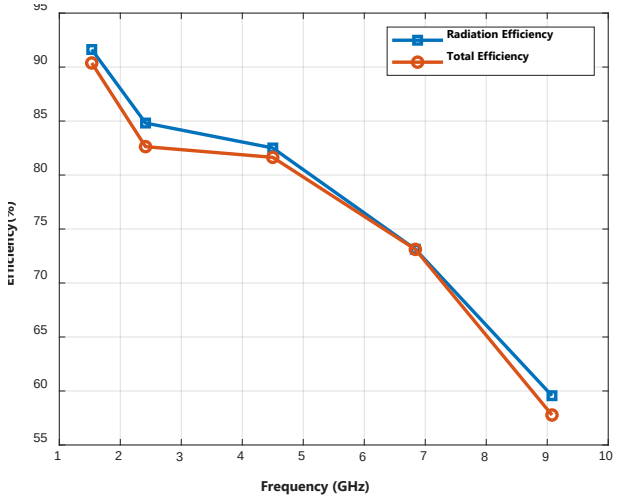

Figure 11. Radiation Efficiency of Proposed Antenna

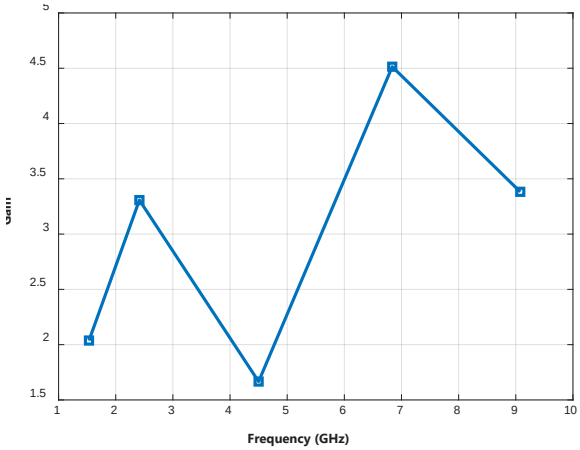

Figure 12. Gain of Antenna

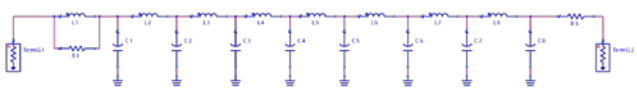

Figure 13. Equivalent circuit of the proposed antenna

VSWR, Gain and Efficiency

The VSWR is below 2, which shows that the maximum energy through the antenna is transmitted. VSWR of the antenna is shown in Figure 10.

Gain of the shows that the transmission of signals in a specific direction. If the gain of an antenna is higher in any specific direction, it shows the antenna has optimal transmission in that direction. If equal or near equal, the antenna is omnidirectional in all directions. The gain of the proposed antenna varies from 1.6 to 4.5 dBi (see Figure 12).

The efficiency of the presented antenna was declined due to dielectric and conductor losses (see Figure 11). The maximum radiation efficiency of the proposed antenna is 91.6%, and the total efficiency is 90.3%.

RLC Components Values

The antenna structure and behaviour can be drawn as an electronic circuit using R, L and C components, called an equivalent circuit. The equivalent circuit of a proposed antenna can be evaluated using a smith chart in CST or ADS software to get the RLC values and their series and parallel connection so that the equivalent return loss characteristics can be reflected. The proposed antenna's equivalent circuit using the ADS is shown in Figure 13. The respective values of RLC components are shown in Table 6. Along with this, RLC values calculated from CST is shown in Table 7.

Table 6. Equivalent RLC Circuit Values from ADS

Components	Values	Components	Values
C_1	*0.229 pF*	L_1	*7.027 nH*
C_2	*0.115 pF*	L_2	*8.207 nH*
C_3	*0.114 pF*	L_3	*8.968 nH*
C_4	*0.331 pF*	L_4	*2.624 nH*
C_5	*0.459 pF*	L_5	*2.997 nH*
C_6	*0.308 pF*	L_6	*3.532 nH*
C_7	*0.895 pF*	L_7	*1.780 nH*
C_8	*0.729 pF*	L_8	*0.132 nH*
R_1	*645.833 ohms*	R_2	*91.731 ohms*

Table 7. RLC Values from CST

Components	Values	Components	Values
R_1	1.8990 ohms	C_7	98.9375 pF
R_2	0.8270 ohms	C_8	778.5684 pF
R_3	1.1460 ohms	C_9	61.3762 pF
R_4	1.3590 ohms	C_{10}	49.6017 pF
R_5	0.5770 ohms	C_{11}	56.3905 pF
R_6	0.8490 ohms	L_1	0.0130 nH
R_7	1.3930 ohms	L_2	0.0118 nH
R_8	0.9940 ohms	L_3	0.0296 nH

R_9	0.6430 ohms	L_4	0.0069 nH
R_{10}	1.0170 ohms	L_5	0.0044 nH
R_{11}	1.4720 ohms	L_6	0.0043 nH
C_1	1138.9199 pF	L_7	0.0093 nH
C_2	880.6325 pF	L_8	0.0007 nH
C_3	211.9263 pF	L_9	0.0054 nH
C_4	617.6313 pF	L_{10}	0.0062 nH
C_5	557.9587 pF	L_{11}	0.0047 nH
C_6	287.4789 pF		

Table 7. Comparison of Performance Metrics of Proposed Antenna

Ref.	Size (mm3)	Impedance BW (GHz)	Peak Gain
[4]	FR4 : 50×50×0.8	2.15-6.97 (4.82)	5 dBi
[5]	FR4 : 60×60×0.8	2.67-13 (10.33)	4.2 dBi
[6]	FR4 : 60×130×0.7	4.24-6.57 (2.33)	5.2 dBi
[7]	FR4: 68×61×1.6	3.4-12 (8.6)	5 dBi
Proposed	FR4 : 60×71.5×1.6	1.294 - 11.248 (9.954)	4.5 dBi

CONCLUSION

The proposed diamond-shaped compact antenna with a large band of operation has been depicted in this research work. The antenna has a 147% (simulated) and 147.88% (measured) fractional bandwidth. This clearly shows the usability of antennas for ultra-wideband operations. The proposed antenna has been simulated on three different software to get the most insights from the antenna geometry. This also gives a different perspective of the real-time scenarios. The theoretical evaluation for validation of return loss resonating frequencies generation has 6.3%, 5.2%, 10%, 8.4%, and 1.74% errors, respectively, for first to fifth resonance. The antenna has shown gain up to 4.5 dBi better for wideband operations. The total efficiency is 90.3% of the antenna, which shows the maximum power radiated from the antenna. These outcomes show the optimal operation of the antenna in ultrawideband applications like 5G, WLAN, WiMAX, Bluetooth, including S-band, C-band and X-Bands applications.

Conflict of Interest

Authors declared no conflict of interest.

REFERENCES

1. Lei Zhu, Sheng Sun, W. Menzel. Ultra-wideband (UWB) bandpass filters using multiple-mode resonator. *IEEE Microwave and Wireless Components Letters* **2005**, 15 (11), 796–798.
2. Dang Trang Nguyen, Dong Hyun Lee, Hyun Chang Park. Very Compact Printed Triple Band-Notched UWB Antenna With Quarter-Wavelength Slots. *IEEE Antennas and Wireless Propagation Letters* **2012**, 11, 411–414.
3. R. Azim, M.T. Islam. Compact Planar UWB Antenna with Band Notch Characteristics For Wlan and DSRC. *Progress in Electromagnetics Res.* **2013**, 133, 391–406.
4. T. Chen, J. Zhang, W. Wang. A Novel CPW-Fed Planar Monopole Antenna with Broadband Circularly Polarization. *Progress in Electromagnetics Res. M* **2019**, 84, 11–20.
5. J. Pourahmadazar, C. Ghobadi, J. Nourinia, N. Felegari, H. Shirzad. Broadband CPW-Fed Circularly Polarized Square Slot Antenna With Inverted-L Strips for UWB Applications. *IEEE Antennas and Wireless Propagation Letters* **2011**, 10, 369–372.
6. T. Saeidi, I. Ismail, W.P. Wen, A.R.H. Alhawari, A. Mohammadi. Ultra-Wideband Antennas for Wireless Communication Applications. *Int. J. Antennas Propagation* **2019**, 2019, 1–25.
7. R.V.R. Krishna, R. Kumar, N. Kushwaha. An UWB dual polarized microstrip fed L-shape slot antenna. *Int. J. Microwave and Wireless Technologies* **2016**, 8 (2), 363–368.
8. R. Azim, A.M.H. Meaze, A. Affandi, et al. A multi-slotted antenna for LTE/5G Sub-6 GHz wireless communication applications. *Int. J. Microwave and Wireless Technologies* **2021**, 13 (5), 486–496.
9. S. Chilukuri, K. Dahal, A. Lokam. Multi-port Pattern diversity antenna for K and Ka-band application. *Advanced Electromagnetics* **2018**, 7 (2), 5–9.
10. T. Sarkar, A. Ghosh, S. L. L. K., S. Chattopadhyay. Notched Integrated Planar Antenna for UWB Application. In *SSRN Electronic Journal*; SSRN, INDIA, **2021**; pp 1–5.
11. T. Kumar, A.R. Harish. Broadband Circularly Polarized Printed Slot-Monopole Antenna. *IEEE Antennas and Wireless Propagation Letters* **2013**, 12, 1531–1534.
12. K. Ding, C. Gao, Y. Wu, D. Qu, B. Zhang. A Broadband Circularly Polarized Printed Monopole Antenna With Parasitic Strips. *IEEE Antennas and Wireless Propagation Letters* **2017**, 16, 2509–2512.
13. M. Midya, S. Bhattacharjee, M. Mitra. Broadband Circularly Polarized Planar Monopole Antenna With G-Shaped Parasitic Strip. *IEEE Antennas and Wireless Propagation Letters* **2019**, 18 (4), 581–585.
14. Q. Chen, H. Zhang, L.-C. Yang, B. Xue, X.-L. Min. Broadband CPW-Fed Circularly Polarized Planar Monopole Antenna with Inverted-L Strip and Asymmetric Ground Plane for WLAN Application. *Progress in Electromagnetics Res C* **2017**, 74, 91–100.
15. Z. An, M. He. A Simple Planar Antenna for Sub-6 GHz Applications in 5G Mobile Terminals. *ACES Journal* **2020**, 35 (1), 10–15.
16. A.K. Arya, S.J. Kim, S. Kim. A Dual-Band Antenna for LTE-R And 5G Lower Frequency Operations. *Progress in Electromagnetics Res. Letters* **2020**, 88, 113–119.
17. N. Sekeljic, Z. Yao, H.-H. Hsu. 5G Broadband Antenna for sub-6 GHz Wireless Applications. In *2019 IEEE International Symposium on Antennas and Propagation and USNC-URSI Radio Science Meeting*; IEEE, Atlanta, GA, USA, **2019**; pp 147–148.
18. G. Jin, C. Deng, J. Yang, Y. Xu, S. Liao. A New Differentially-Fed Frequency Reconfigurable Antenna for WLAN and Sub-6GHz 5G Applications. *IEEE Access* **2019**, 7, 56539–56546.
19. T. Kiran, N. Mounisha, C. Mythily, D. Akhil. Design of Microstrip Patch Antenna for 5g Applications. *IOSR Journal of Electronics and Communication Engineering* **2018**, 13 (1), 14–17.
20. R. Azim, M.T. Islam, N. Misran. Microstrip Line-fed Printed Planar Monopole Antenna for UWB Applications. *Arabian Journal for Science and Engineering* **2013**, 38 (9), 2415–2422.

21. A.K. Chaudhary, M. Manohar. Design And Analysis of A Compact High Gain Wideband Monopole Patch Antenna for Future Handheld Gadgets. *Progress in Electromagnetics Res. C* **2021**, 109, 227–241.
22. A. Dastranj, F. Ranjbar, M. Bornapour. A New Compact Circular Shape Fractal Antenna For Broadband Wireless Communication Applications. *Progress in Electromagnetics Res C* **2019**, 93, 19–28.
23. A.A. Kadam, A.A. Deshmukh. Pentagonal Shaped UWB Antenna Loaded with Slot and EBG Structure for Dual Band Notched Response. *Progress in Electromagnetics Res. M* **2020**, 95, 165–176.
24. A. Kumar, A.A. Althuwayb, M.J. Al-Hasan. Wideband Triple Resonance Patch Antenna for 5G Wi-Fi Spectrum. *Progress in Electromagnetics Res Letters* **2020**, 93, 89–97.
25. Y. Liu, H. Wang, X. Dong. Design of A Dual-Polarized Broadband Single-Layer Reflectarray Based On Square Spiral Element. *Progress in Electromagnetics Res. M* **2018**, 72, 23–30.
26. B. Lokeshwar, D. Venkatasekhar, J. Ravindranadh. Development of A Low-Profile Broadband Cavity Backed Bow-Tie Shaped Slot Antenna in SIW Technology. *Progress in Electromagnetics Res. Letters* **2021**, 100, 9–17.
27. N. Ojaroudi Parchin, H.J. Basherlou, R.A. Abd-Alhameed. UWB Microstrip-Fed Slot Antenna with Improved Bandwidth and Dual Notched Bands using Protruded Parasitic Strips. *Progress in Electromagnetics Res. C* **2020**, 101, 261–273.
28. H. Paik, L.C. Teja, M. Akash Reddy, K. Sai Trinadh Reddy. A Miniaturized Fractal Antenna with Square Ring Slots For Ultrawideband Applications. *Progress in Electromagnetics Res. Letters* **2021**, 99, 169–177.
29. J.H. Wang. Dual Band-Notched UWB Antenna with Improved Radiation Pattern. *Progress in Electromagnetics Res. C* **2020**, 103, 59–70.
30. J. Yeo. Miniaturized UWB Stepped Open-Slot Antenna. *Progress in Electromagnetics Res. Letters* **2018**, 78, 119–127.